

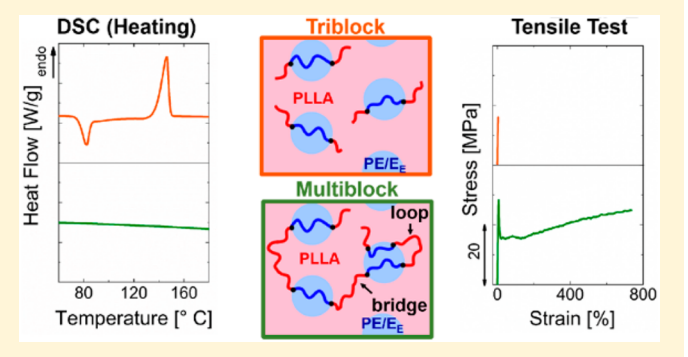
Crystallization and Mechanical Properties of Poly(L-lactide)-Based Rubbery/Semicrystalline Multiblock Copolymers

Tessie R. Panthani and Frank S. Bates*

Department of Chemical Engineering and Materials Science, University of Minnesota, Minnesota, Minnesota 55455, United States

Supporting Information

ABSTRACT: The crystallization and mechanical properties of triblock and multiblock copolymers containing 70 vol % semicrystalline poly(L-lactide) (L) and 30 vol % rubbery poly(ethylene-co-ethylene) (E/E_E) were investigated. The multiblock copolymer was synthesized directly from the triblock copolymer (denoted LE/E_EL). Specifically, the dihydroxyl-terminated LE/E_EL served as a macromonomer in a step-growth polymerization in which stoichiometric quantities of sebacoyl chloride were added, resulting in (LE/ $E_E L$)_(3.6), a multiblock copolymer with an average of 3.6 triblock copolymer units connected together. Additionally, triblock and multiblock copolymers were blended together in



order to systematically tune $\langle n \rangle$ and uncover the role of block number on properties. Dynamic mechanical analysis (DMA) indicated that despite differences in $\langle n \rangle$, all samples had an order-to-disorder transition temperature $T_{\rm ODT} \approx 190$ °C, which is above the melting temperature (T_m) of poly(L-lactide). Small-angle X-ray scattering measurements (SAXS) of the block copolymers at $T_{\rm m} < T < T_{\rm ODT}$ showed that the samples had identical morphology (hexagonally packed cylinders) and domain spacing. Isothermal crystallization experiments were performed using differential scanning calorimetry (DSC) and indicated that samples with higher $\langle n \rangle$ had a lower percentage crystallinity after 1 h of crystallization, which we associate with the differences in the average chain architecture. Uniaxial tensile measurements demonstrate a brittle-to-ductile transition at $\langle n \rangle = 1.8$ for specimens with limited crystallinity. Finally, the effect of crystallinity on mechanical properties was investigated by annealing select samples.

INTRODUCTION

Block polymers are an intriguing and useful class of materials due to the ability to precisely tune morphology and properties by changing parameters including composition, molecular weight, and block sequencing.1 While diblock and triblock copolymers have been studied extensively in the literature, fewer reports have focused on multiblock copolymers. Interestingly, multiblock copolymers have been shown to have superior mechanical properties relative to diblock and triblock copolymers due to the ability of these molecules to bridge multiple nanoscale domains. 2-11 For this reason, incorporating brittle poly(lactide) (PLA) into a multiblock copolymer architecture is an attractive option for improving its mechanical properties. Additionally lactide, as well as other renewable cyclic esters such as β -methyl- δ -valerolactone, ¹² menthide, ¹³ ε -decalatone, ⁹ and δ -decalactone, ¹⁴ can be polymerized with α,ω -dihydroxyl functionality by using difunctional alcohols as initiators. Hence, sustainable-based multiblock copolymers can be prepared from homopolymer and block polymer macromonomers by step-growth methods using difunctional isocyanates and acid chlorides, among other approaches. 4,15-20 Because of the potential to improve mechanical properties and the simple synthetic routes,

multiblock copolymers are poised to play an important role in developing the next generation of sustainable polymers.

Introducing a crystallizable component into a block copolymer architecture has consequences on the morphology, ^{21–23} crystallization kinetics, ^{24,25} and mechanical properties. ^{26–30} For instance, the morphology of a block copolymer system after crystallization of one of the blocks is dictated by the relative thermal transitions in the material. When the melting temperature $(T_{\rm m})$ of the crystallizable block exceeds both the order-to-disorder transition temperature (T_{ODT}) and the glass transition temperature of the amorphous block (T_{gamorph}) , crystallization proceeds from the homogeneous In this case, crystallization can induce microphaseseparated structures since the noncrystallizable block is expunged from the crystallized domains. On the other hand, if the T_{ODT} exceeds the T_{m} of the crystallizable block, the sample will order before crystallizing, and upon further cooling, the ordered morphology may be preserved after crystallization. For example, if $T_{\rm g,amorph}$ is above the crystallization temperature $(T_{\rm g,amorph} > T_{\rm c})$, crystallization is forced to occur within the hard

Received: May 13, 2015 Revised: June 12, 2015 Published: June 22, 2015

walls of the glassy block. $^{32-35}$ Conversely, if $T_{\rm g,amorph} < T_{\rm O}$ the situation is more complicated. When the segregation strength is high, crystallization has been shown to be confined to the microphase-separated domains. 36,37 In cases when the segregation strength is relatively weak, however, it is known that crystallization can disrupt the melt morphology as discussed in detail by Loo and co-workers. 21 Furthermore, block copolymers which order via crystallization-induced microphase separation have been shown to have different mechanical behavior than similar samples which crystallize in the ordered melt. 6

In our recent work, we reported the synthesis and characterization of triblock and multiblock copolymers composed of glassy poly(DL-lactide) (PDLLA) and rubbery poly(butadiene) (PB) blocks.4 The multiblock copolymers were synthesized by simple step-growth polymerization of the telechelic $\alpha_i\omega$ -dihydroxy-terminated triblock copolymers. Detailed characterization revealed that the multiblock copolymers had identical morphologies as the triblock copolymer precursors. Yet in nearly all instances, the multiblock copolymer was found to be significantly tougher and more ductile than the triblock copolymer precursor, suggesting that the improvements in mechanical properties were due to the change in architecture. From a commercialization standpoint, one shortcoming of this system is that the material had a low upper service temperature (UST) due to the relatively low glass transition temperature of the PDLLA block ($T_{\rm g}$ = 57 °C in the high molecular weight limit).³⁸ In this work, we expand on these results by studying similar materials with two significant modifications. First, glassy PLA is replaced with semicrystalline poly(L-lactide) (PLLA). Utilizing PLLA is particularly enticing for the application of tough, sustainable plastics since it has an equilibrium melting temperature $T_{\rm m}^{\infty}$ of ≈ 180 °C and thus has a higher UST than glassy PDLLA.³⁹ Second, to prevent undesired cross-linking of the material, the PB block employed in our previous work is replaced with a hydrogenated PB or poly(ethylene-co-ethylethylene) (PE/E_E). (PE/E_E is our nomenclature for this material, which is synthesized by Cray Valley and marketed as Hydrogenated Krasol resin.) A PLLA-PE/E_E-PLLA (denoted LE/E_EL) triblock copolymer containing 70 vol % PLLA was synthesized using ring-opening polymerization. The triblock was then chain extended to a multiblock copolymer using sebacoyl chloride as a coupling agent. A series of triblock/multiblock copolymer blends were prepared in order to probe the effect of chain architecture on crystallization and mechanical properties.

EXPERIMENTAL SECTION

Synthesis of Poly(L-lactide-b-ethylene-co-ethylethylene-b-Llactide) (LE/E_EL) Triblock Copolymer. LE/E_EL triblock copolymer was synthesized via ring-opening polymerization using commercially available \alpha,\omega-dihydroxy hydrogentated polybutadiene (HO-PE/E_E-OH) (KRASOL HLBH-P 2000, Cray Valley USA, LLC) in a similar manner as described previously.4 The HO-PE/E_E-OH served as the macroinitiator for the polymerization of L-lactide. HO-PE/E_E-OH was poured into a pressure flask containing a stir bar and was stirred overnight under dynamic vacuum to remove air and any residual solvent. The flask was then transferred into a drybox. Here, L-lactide and tin(II) octoate (0.1% relative to monomer) were added to the flask. In addition, dry toluene was added to the flask to make a 30 wt % solution. (The toluene used here was previously dried by passing the solvent through activated alumina columns before collecting in a flame-dried flask.) The pressure flask was then removed from the drybox and placed in an oil bath at 70 °C for 30 min while stirring. The temperature was then raised to 105 °C, and the solution was stirred at this temperature for 3.5 h. Finally, the flask was submerged in ice water to quench the reaction, and the contents of the flask were then precipitated in cold methanol. The precipitated polymer was recovered by decanting the excess methanol followed by drying under vacuum. $^1\mathrm{H}$ NMR spectroscopy revealed that the L-lactide polymerization reached >99% conversion and resulted in a polymer with a number-average molecular weight (M_n) of 10 500 g/mol and a composition of 70 vol % PLLA $(f_\mathrm{PLLA}=0.7)$.

Synthesis of Multiblock Copolymer. The multiblock copolymer was synthesized by coupling the previously synthesized $LE/_EL$ triblock via a polycondensation reaction with sebacoyl chloride. First, LE/E_EL was added to the pressure flask and dried under vacuum overnight. The flask containing the polymer was the brought into a drybox, and a stoichiometric amount of sebacoyl chloride was added. In addition, equal volumes of pyridine and toluene were added to the flask to make a 20 wt % solution. Pyridine served as both a catalyst and solvent for the reaction. The pyridine utilized here was previously dried by stirring over sodium hydroxide pellets for 2 weeks followed by vacuum distillation to a flame-dried flask. The toluene was dried as described in the previous section.

Preparation of Triblock/Multiblock Copolymer Blends. Blends of the synthesized triblock and multiblock copolymers were prepared in order to elucidate the role of block number on the crystallization and mechanical properties. The blends were prepared by codissolution in benzene followed by freeze-drying. First, the triblock and multiblock copolymers were weighed and placed in round-bottom flask containing a stir bar. Benzene was then added to the flask to make ∼10 wt % solutions. The mixture was stirred until the polymer was completely dissolved then the polymer/benzene solutions were frozen using liquid nitrogen. The flasks were connected to a vacuum line, and the contents of the flask were maintained under dynamic vacuum until the line reached baseline.

Molecular Characterization. The molecular weight and block compositions of LE/E_EL triblock copolymers were determined using ¹H nuclear magnetic resonance (NMR) spectroscopy. The sample was dissolved into deuterated chloroform (CDCl₃, Cambridge Isotope Laboratories, Inc.) and measured with a Varian Inova 500 spectrometer at room temperature. The molecular weight and mole fraction was calculated by end-group analysis. The volume fractions were converted from mole fractions using the published homopolymer densities ($\rho_{\rm PLA}=1.27,~\rho_{\rm E/EE}=0.860$). Size exclusion chromatography (SEC) was used to obtain the number-average molecular weight (M_n) , weight-average molecular weight (M_w) , and dispersity (D) of the triblock and multiblock copolymers as well as the blends. SEC analyses were performed on a Thermo Separation Products (TSP) Spectra Systems AS1000 autosampler equipped with three 5 mm Phenomenex Phenogel columns, a Waters 515 pump, and a Waters 2410 differential refractive index detector. The samples were run with THF (Sigma-Aldrich) as a carrier solvent at room temperature. The reported molecular weights were determined based on using a calibration with 10 polystyrene standards (580-377 400 g/mol, Polymer Laboratories)

Dynamic Mechanical Analysis (DMA). The order-to-disorder transition temperatures $(T_{\rm ODT}s)$ of the triblock and multiblock copolymers and the associated blends were determined by DMA using a Rheometrics Scientific strain-controlled ARES rheometer. For the multiblock copolymer and blends, measurements were obtained using 8 mm parallel plates. Measurements were taken using 50 mm parallel plates for the triblock copolymer. Samples were first loaded at 180 °C. Strain sweeps were conducted at 180 °C to determine the linear viscoelastic regime. All experiments were conducted at a strain which was determined to be in the linear viscoelastic regime for each sample. For isochronal temperature ramps, the elastic (G') and storage (G'') moduli were monitored at a constant frequency (1 rad/s) while heating samples at a constant rate (2 °C/min). For isothermal frequency sweeps, samples were annealed at each temperature for 5 min prior to data collection.

Differential Scanning Calorimetry (DSC). Thermal transitions were determined using a Thermal Analysis Q1000 DSC. Samples were

loaded into hermetically sealed aluminum DSC pans, heated to 200 $^{\circ}$ C, cooled to -115 $^{\circ}$ C, and reheated to 200 $^{\circ}$ C at a rate of 10 $^{\circ}$ C/min. The glass transition and melting temperatures was obtained during the second heating step.

Isothermal Crystallization by DSC. Differences in the crystallization behavior of the triblock and multiblock copolymers, as well as their blends, were probed by isothermal crystallization experiments. Samples were loaded into hermetically sealed aluminum DSC pans and heated to $T_{\rm anneal} = 180~{\rm C}~(T_{\rm m} < T_{\rm anneal} < T_{\rm ODT})$ and held at this temperature for 10 min. Subsequently, the samples were quenched at a rate of 60 °C/min to a crystallization temperature, $T_{\rm c}$ which was varied between 90 and 130 °C. Samples were held at $T_{\rm c}$ for either 1 or 3 h. Finally, samples were rapidly heated at a rate of 60 °C/min to 180 °C to melt any crystals that may have formed during the crystallization process. An additional set of samples underwent the isothermal crystallization procedure at $T_{\rm c} = 100~{\rm ^{\circ}C}$ for 1 h, followed by a rapid quench to $T < T_{\rm g,PLLA}$ in order to vitrify the sample so that the morphology of the crystallized samples could be preserved and investigated at a later time with small-angle X-ray scattering (SAXS).

Small-Angle X-ray Scattering (SAXS). Synchrotron source SAXS measurements were taken at Argonne National Laboratory (Argonne, IL). High temperature (180 °C) and room temperature SAXS data were recorded with an X-ray energy of 14 keV ($\lambda=0.856$ Å) and 17 keV ($\lambda=0.729$ Å), respectively. In both cases, the collected two-dimensional scattering data were azimuthally integrated and are presented as intensity (I) vs scattering wave vector, $q=(4\pi/\lambda)\sin(\theta/2)$, where θ is the scattering angle.

Transmission Electron Microscopy. Polymer samples were prepared for TEM by first hot pressing at ~ 170 °C and quenching the temperature of the press to room temperature using cooling water. The pressed samples were then trimmed with a razor blade to form a flat surface and stained with the vapor of an aqueous solution of ruthenium tetroxide (RuO₄) solution for 4 h. RuO₄ preferentially stains the rubbery PE/E_E domains, providing contrast for imaging. Stained samples were then cut into thin slices (80–100 nm thickness) using a Leica UC6 microtome operated at room temperature and placed on copper grids. TEM data were obtained using a FEI Tecnai Spirit electron microscope at College of Science and Engineering Characterization Facility at the University of Minnesota.

Tensile Testing. Uniaxial tensile tests were conducted with a RSA-G2 solids analyzer (TA Instruments) at room temperature. Polymer films with thickness of about 0.2 mm were prepared using a hot press at \sim 170 °C for 2 min, followed by quenching the samples to 50 °C at a cooling rate of approximately 35 °C/min. In addition, two samples were annealed to enhance crystallinity; these samples were hot pressed at \sim 170 °C for 2 min and cooled to 50 °C, removed from the press, and left at ambient temperature for 30 min. Subsequently, the samples were pressed at 100 °C for 30 min, followed by quenching to 50 °C with cooling water. For all samples, dog-bone specimens were made from the films using a punch and arbor press with the following dimensions: total length (25 mm), gauge length (6 mm), cross-section width (3.2 mm), and thickness (approximately 0.2 mm). The samples were stored at room temperature for about 48 h after pressing prior to testing. Specimens were drawn until failure with a constant rate of 0.1 mm/s. Engineering stress ($\sigma = F/A_0$) was calculated from the force (F) and the initial cross-sectional area (A_0) ; the nominal strain $(\varepsilon = (l (l_0)/l_0$) was determined from the change in grip-to-grip distance $(l-l_0)$ and the initial gauge length (l_0) . Young's modulus (E) was obtained from the slope of the linear regime of the stress-strain curve. At least five specimens were tested for each sample and averaged for all data reported here.

■ RESULTS AND DISCUSSION

Synthesis and Molecular Characterization. Six materials composed of semicrystalline poly(L-lactide) (PLLA or L) and rubbery poly(ethylene-co-ethylethylene) (PE/ E_E or E/ E_E) were studied in this work: a triblock copolymer, multiblock copolymer, and four triblock/multiblock copolymer blends. Two different parameters are utilized to characterize the

samples: $\langle n \rangle$ (the average number of connected triblock copolymers in each sample) and $w_{\rm triblock}$ (the weight fraction of triblock in each sample). Table 1 lists the values of $\langle n \rangle$ and $w_{\rm triblock}$ for each sample as well as other important molecular characteristics.

Table 1. Molecular Characteristics LE/E_EL Triblock and $(LE/E_EL)_{(3.6)}$, Multiblock Copolymer and Triblock/Multiblock Copolymer Blends

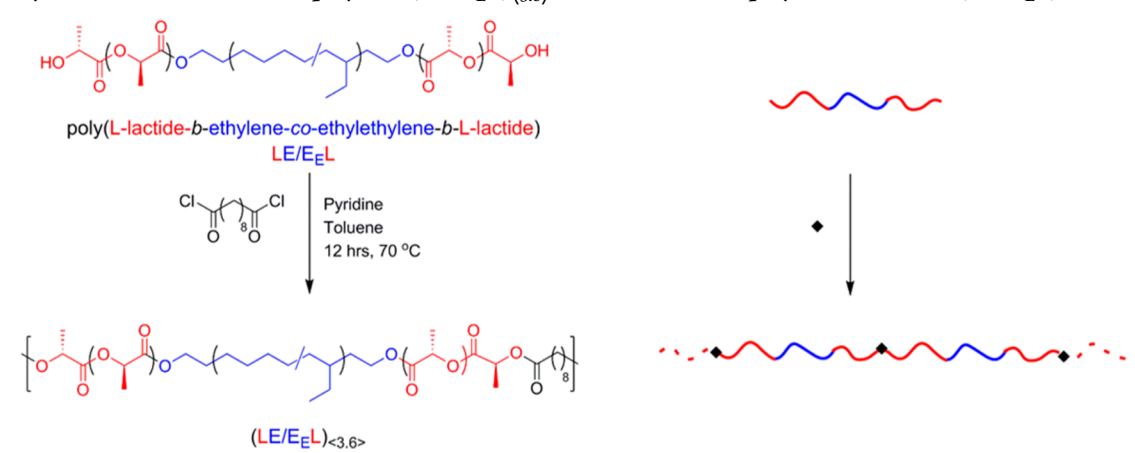
sample	$M_{\rm n} angle ({ m kg/mol})$	\mathcal{D}^c	f_{PLLA}^{d}	$\langle n \rangle^e$	$\langle n' \rangle^f$	$w_{\mathrm{triblock}}^{g}$
triblock						
LE/E_EL	10.5 ^a	1.08	0.7	1	3.0	1
multiblock						
$(LE/E_EL)_{\langle 3.6\rangle}$	37.8 ^b	2.63	0.7	3.6	8.2	0
blends						
$(LE/E_EL)_{\langle 1.4 \rangle}$	14.6 ^b	2.86	0.7	1.4	3.8	0.60
$(LE/E_EL)_{\langle 1.8 \rangle}$	19.3 ^b	3.08	0.7	1.8	4.7	0.41
$(LE/E_EL)_{\langle 2.4\rangle}$	24.9 ^b	2.81	0.7	2.4	5.7	0.21
$(LE/E_EL)_{\langle 2.9\rangle}$	31.0^{b}	2.30	0.7	2.9	6.9	0.10

"Number-average molecular weight (M_n) of the triblock copolymer calculated from ¹H NMR analysis. bM_n of multiblock copolymer and blends determined by multiplying $\langle n \rangle$ by the M_n determined for LE/E_EL by ¹H NMR end-group analysis. ^cDispersity (D) measured by SEC. ^dVolume fraction of PLLA $(f_{\rm PLLA})$ measured by ¹H NMR and calculated using published bulk homopolymer densities. ^{40,41} ^eAverage number of triblock copolymers in multiblock copolymer $(\langle n \rangle)$ calculated from SEC-measured molecular weights. ^fAverage number of total blocks in each sample $(\langle n' \rangle)$ is calculated by the following formula: $\langle n' \rangle = 2\langle n \rangle + 1$. ^gWeight fraction of triblock copolymer $(w_{\rm triblock})$ in each sample.

All samples had an asymmetric composition of $f_{PLLA} = 0.7$ (where f_{PLLA} is the volume fraction of PLLA in the sample). The triblock copolymer, composed of a PE/E_E midblock and PLLA end blocks, was synthesized in a similar manner as in our previous work.⁴ The multiblock copolymer (LE/E_EL)_(3.6) was prepared by a polycondensation reaction of the dihydroxylterminated LE/E_EL with sebacoyl chloride, as illustrated in Scheme 1. For the multiblock copolymers and blends, the subscript in the sample name is equal to $\langle n \rangle$. (The average number of total blocks, $\langle n' \rangle$, can be calculated by the simple formula $\langle n' \rangle = 2 \langle n \rangle + 1$). Figure 1 shows size exclusion chromatography (SEC) traces for the triblock and multiblock copolymers. While LE/E_EL has a fairly narrow molecular weight distribution (D < 1.10), the molecular weight distribution of (LE/E_EL)_(3.6) is predictably broad (D > 2), as expected from a step-growth polymerization technique. In order to vary $\langle n \rangle$, a series of blends were made by mixing the triblock and multiblock copolymers. Figure 1 also shows size exclusion chromatography (SEC) traces from blends of triblock and multiblock copolymers with $\langle n \rangle$ ranging from 1.4 to 2.9.

Order-to-Disorder Transition and Morphology. Order-to-disorder transition temperatures ($T_{\rm ODT}$ s) where determined using dynamic mechanical analysis (DMA) measurements. Isochronal temperature ramps ($\omega=1$ rad/s) were taken for all samples while heating at a rate of 2 °C/min; all samples were annealed at 180 °C for 10 min prior to measurement. Figure 2 shows representative temperature ramps in which G' is monitored as a function of temperature. The order-to-disorder transition is taken to occur at the temperature at which G' drops abruptly as indicated with arrows. Despite the difference in $\langle n \rangle$ of these samples, the $T_{\rm ODT}$ is evident over a narrow

Scheme 1. Synthesis of Multiblock Copolymer (LE/E_EL)_(3.6) from Triblock Copolymer Precursor (LE/E_EL)



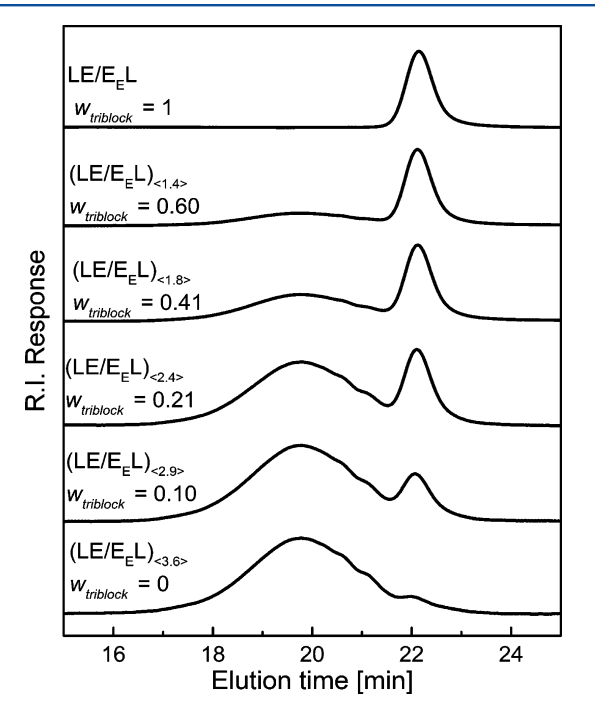


Figure 1. SEC traces of LE/E_EL (triblock copolymer), (LE/E_EL)_(3.6), and triblock/multiblock copolymer blends. Weight fraction of triblock, w_{triblock} is indicated for each sample.

temperature range (188–191 °C). The effect of architecture on the T_{ODT} has been discussed by Wu and co-workers in their work on symmetric multiblock copolymers. 42 Using a generalized random phase approximation (RPA) theory, they determined that for symmetric multiblock copolymers T_{ODT} should increase with increasing n' but asymptotically approaches a limiting value for $n' \gg 1$, which was verified experimentally. (Here, the notation n' is used instead of $\langle n' \rangle$ to emphasize that the materials in the previous study had a precise number of blocks per sample.) The fact that our samples have nearly identical apparent T_{ODT} values is interesting and may be a consequence of the heterogeneous mixture of architectures in these materials. Mori et al. studied the T_{ODT} of CEC/CECEC blends (where "C" is poly(cylcohexylethylene) and "E" is poly(ethylene)) and found a nonlinear relationship between the weight fraction of pentablock in the blends and the $T_{\rm ODT}$. ⁴³ They found that within experimental error all samples composed of 0-30 wt % pentablock copolymer had identical

 $T_{\rm ODT}$ s. This helps explain the invariant $T_{\rm ODT}$ observed in the LE/E_EL/(LE/E_EL)_(3.6) system. The pure multiblock copolymer material, (LE/E_EL)_(3.6), contains a small amount of residual triblock copolymer (~5 wt %), as evidenced by the low molecular weight shoulder visible in the SEC trace in Figure 1, which may contribute to depression of the $T_{\rm ODT}$. Notwithstanding, the invariant $T_{\rm ODT}$ is useful in practice since it lowers the required processing temperature of the multiblock copolymer.

Small-angle X-ray scattering (SAXS) patterns taken at 180 °C are shown in Figure 3. All samples shows a sharp principal reflection (q^*) along with one or more scattering reflections at higher q. The relative q/q^* values reveal that these samples have hexagonal symmetry with higher order reflections at characteristic values of $q/q^* = 1$, $3^{1/2}$, $4^{1/2}$, and $7^{1/2}$. Based upon the volume fraction ($f_{\rm PLLA}$ = 0.7), these samples are most likely composed of hexagonally packed cylinders of PE/E_E in a PLLA matrix. This conclusion is supported by TEM images obtained from the triblock and pure multiblock; a representative set of images are shown in Figures 3b and 3c. While microphase separation in diblock or triblock copolymers is almost always associated with long-range periodic order, this is not necessarily true for multiblock copolymers. In fact, microphase-separated structures with long-range disorder have been observed in other multiblock copolymer systems 15,44 and are exclusively observed in related polyurethane materials. 45–47 It is unclear whether the lack of long-range order in these other studies is due to entropic or kinetic factors associated with increasing the number the blocks and is an interesting topic worthy of further investigation. Nevertheless, it appears that our system falls in a $\langle n \rangle$ regime where access to long-range order is quite facile. All samples have a nearly identical $D^* = 9.8 \pm 0.1$ nm. This is in contrast to studies on $(SIS)_n$ multiblock copolymers, where D^* increased with n. ^{42,48} This discrepancy, however, is likely due to the fact that in the (SIS)_n samples the T_{ODT} increases with n. Thus, at any temperature below the T_{ODT} , the segregation strength is higher for samples with higher n, resulting in a higher degree of chain stretching and subsequently larger D^* . In the LE/E_EL/(LE/E_EL)_(3.6) system, the $T_{\rm ODT}$ does not change with $\langle n \rangle$, thereby decoupling D^* from $\langle n \rangle$.

Crystallization and Melting Behavior. Figure 4 shows representative DSC heating traces obtained during the second heating step. Additional information about the thermal properties, including glass transition temperatures $(T_{\rm g})$ and the peak melting temperature $(T_{\rm m})$, were extracted from these

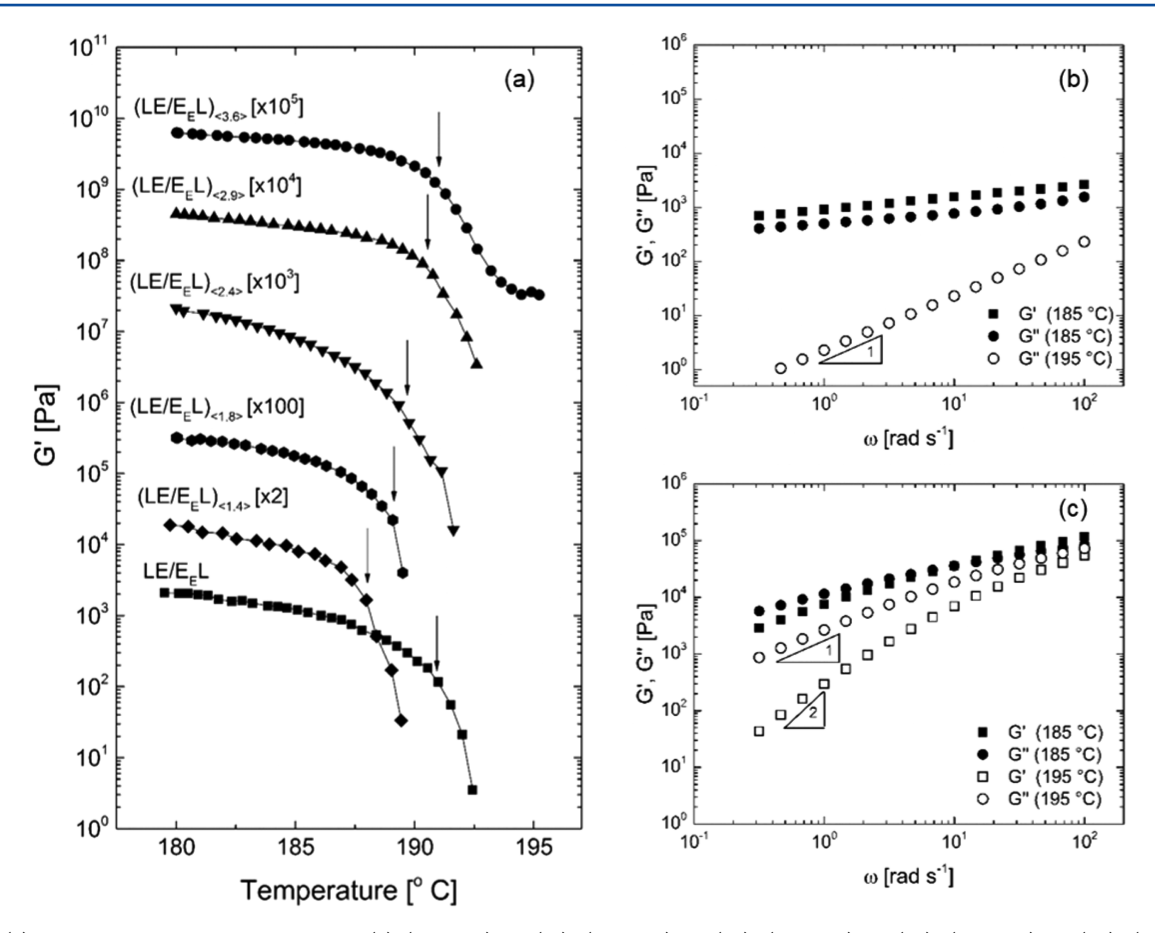


Figure 2. (a) Isochronal temperature ramp data: (a) $(LE/E_EL)_{\langle 3.6 \rangle}$ (\spadesuit), $(LE/E_EL)_{\langle 2.9 \rangle}$ (\spadesuit), $(LE/E_EL)_{\langle 2.4 \rangle}$ (\blacktriangledown), $(LE/E_EL)_{\langle 1.8 \rangle}$ (\spadesuit), $(LE/E_EL)_{\langle 1.4 \rangle}$ (\spadesuit), and LE/E_EL (\blacksquare). (b) Isothermal frequency sweep data for LE/E_EL : G' at 185 °C (\blacksquare), G'' (\spadesuit) at 185 °C, and G'' at 195 °C (\bigcirc). (c) Isothermal frequency sweep data for $(LE/E_EL)_{\langle 3.6 \rangle}$: G' at 185 °C (\blacksquare), G'' (\spadesuit) at 185 °C, G' at 195 °C (\bigcirc), and G'' at 195 °C (\bigcirc).

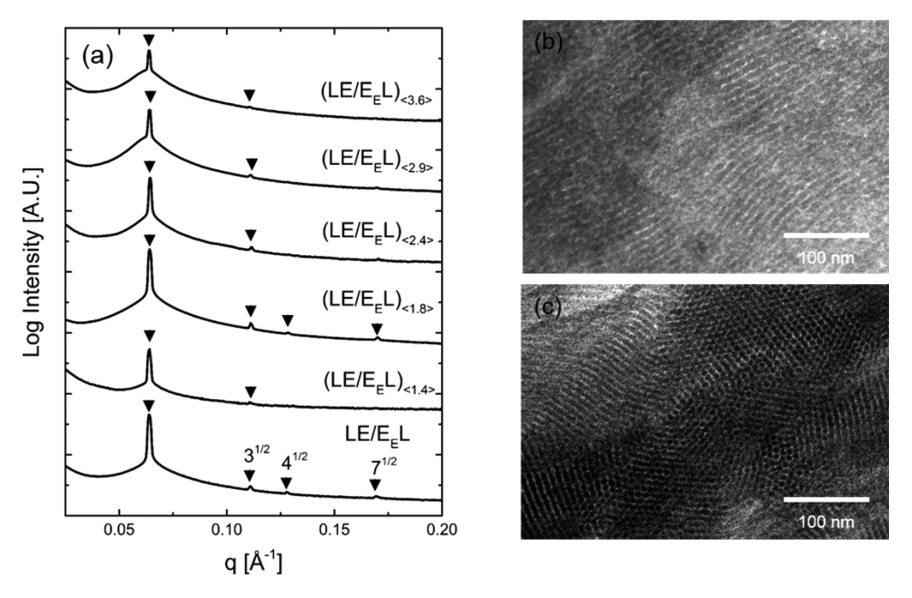


Figure 3. (a) One-dimensional SAXS patterns at 180 °C. Triangles identify Bragg peaks associated with hexagonal order. (b) TEM image of LE/E_EL . (c) TEM image of $(LE/E_EL)_{(3,6)}$. Prior to TEM, samples were heated on a hot press to 170 °C and quenched to room temperature which resulted in samples with negligible crystallinity. TEM specimens were stained with RuO_4 to enhance contrast between the PLLA and PE/E_E domains. These images are consistent with a cylindrical morphology.

experiments and are included in Table 2. Despite similarities in the $T_{\rm ODT}$ and melt structure, these samples clearly have different crystallization behaviors. As LE/E_EL is heated above $T_{\rm g,PLLA}$, the DSC trace first shows an exotherm at ~82 °C,

which can be attributed to the cold crystallization of the PLLA block. Upon further heating, melting of the PLLA crystals is observed with the peak melting temperature $T_{\rm m,peak}$ occurring at about 142 °C. The addition of a small amount of the multiblock

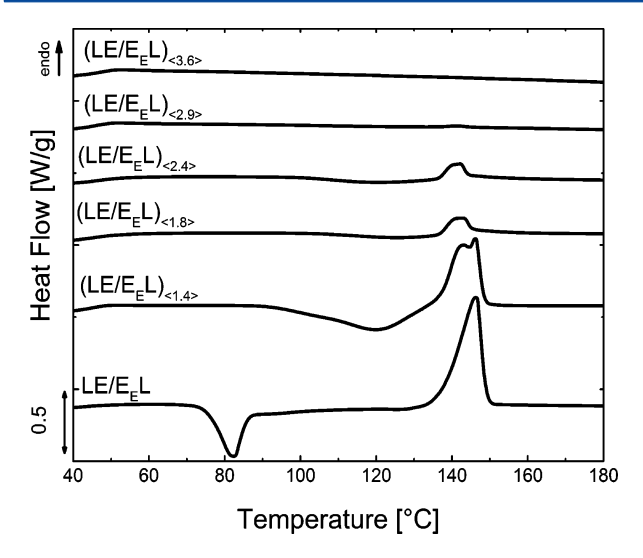


Figure 4. DSC second heating ramp results obtained at 10 °C/min.

Table 2. Summary of Thermal Properties from DSC Second Heating Trace

sample	$T_{\rm g,PLLA}$ (° C)	$T_{\mathrm{g,PE/EE}}$ (° C)	$T_{\rm m}$ (° C)
LE/E_EL	40.2	-48.8	149.6
$(LE/E_EL)_{\langle 1.4 \rangle}$	45.2	-48.9	146.2
$(LE/E_EL)_{\langle 1.8 \rangle}$	45.4	-48.1	142.1
$(LE/E_EL)_{\langle 2.4\rangle}$	47.0	-46.6	142.1
$(LE/E_EL)_{\langle 2.9 \rangle}$	46.5	-50.2	141.4
$(LE/E_EL)_{(3.6)}$	47.1	-46.4	

copolymer to the triblock copolymer (or, equivalently, an increase in $\langle n \rangle$) changes the observed crystallization and melting behavior. The DSC heating trace of (LE/E_EL)_(1.4) shows a broad cold crystallization peak that is shifted to significantly higher temperatures compared to LE/E_EL. A bimodal melting exotherm is also observed after the cold crystallization event. Since the cold crystallization and melting peaks overlap and are difficult to differentiate, it is impossible to interpret the areas of the peaks relative to that for LE/E_EL with certainty. As $\langle n \rangle$ increases further, however, it is clear that the magnitudes of both the cold crystallization and melting peak decrease along with a decrease in $T_{\rm m}$. In the case of (LE/E_EL)_(3.6), neither a crystallization nor melting peak can be resolved

Isothermal crystallization experiments were performed on LE/E_EL and $(LE/E_EL)_{(3.6)}$ to obtain additional information on the crystallization kinetics and subsequent melting behavior of these materials. Samples were annealed at 180 $^{\circ}$ C ($T_{\rm m}$ < T < $T_{\rm ODT}$) for 10 min followed by a rapid quench to a crystallization temperature (T_c) between 90 and 130 °C with samples being held at T_c for 1 or 3 h. Figure 5a shows the crystallization exotherm for LE/ E_E L. For all T_c s investigated, a crystallization exotherm is observed, where the return of the heating trace to the value recorded at t = 0 min indicates that crystallization is completed within 1 h. In contrast, Figure 5b shows that for $(LE/E_EL)_{(3,6)}$ crystallization is not complete after 1 h. To further explore this result, isothermal crystallization experiments also were performed for 3 h at $T_c = 100$, 105, and 110 °C for this sample. The results of these experiments are shown in Figure 5c. (Note that the y-axis of Figure 5c is magnified by a factor of 10 compared to Figures 5a and 5b.)

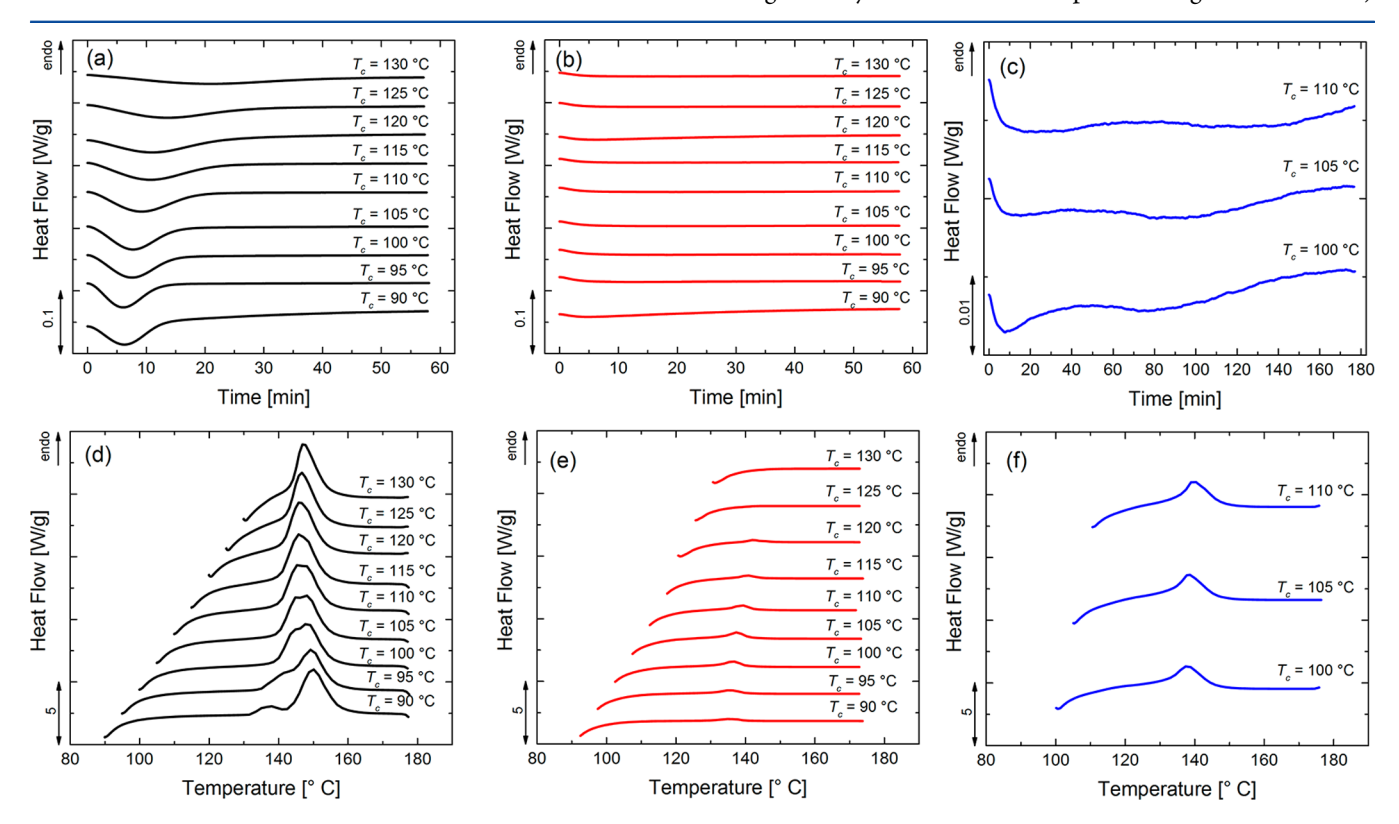
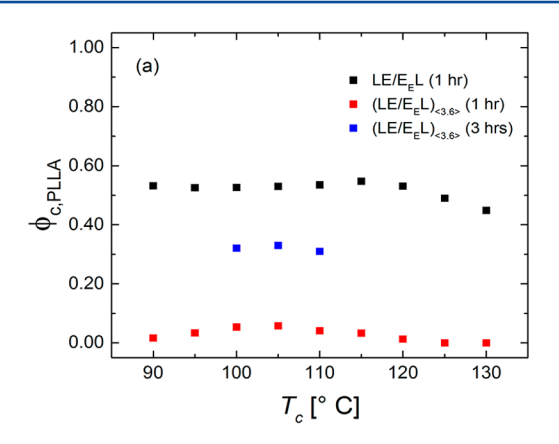


Figure 5. Measured heat flow versus time during isothermal crystallization at various $T_c s$: (a) LE/E_EL crystallized for 1 h and (b) (LE/E_EL)_(3.6) crystallized for 3 h. Measured melting endotherms after isothermal crystallization at various $T_c s$ for (d) LE/E_EL crystallized for 1 h, (e) (LE/E_EL)_(3.6) crystallized for 1 h, and (f) (LE/E_EL)_(3.6) crystallized for 3 h.



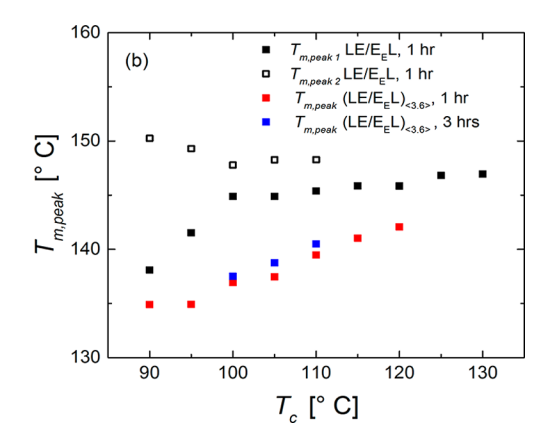
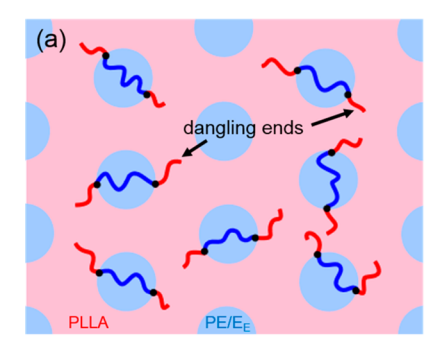


Figure 6. (a) $\Phi_{c,PLLA}$ after isothermal crystallization at various $T_c s$ for 1 or 3 h. (b) $T_{m,peak}$ after isothermal crystallization at various $T_c s$.



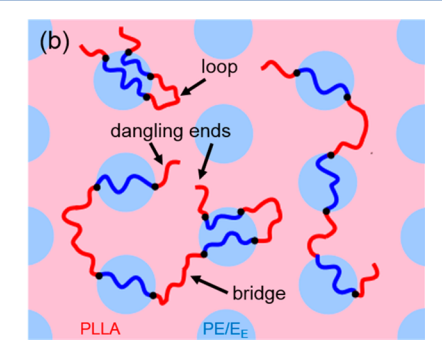


Figure 7. Schematic illustrating chain conformations in (a) LE/E_EL and (b) (LE/E_EL)_(3.6). The interior PLLA blocks in (LE/E_EL)_(3.6) can form bridges and loops while all the PLLA blocks of LE/E_EL are dangling ends.

Unlike LE/E_EL, (LE/E_EL)_(3.6) has two distinct exothermic peaks in the measured heat evolution during the crystallization experiment, suggesting that this sample crystallizes by two different mechanisms, a point that we return to later. Interestingly, the first peak of the crystallization exotherm occurs at approximately the same time ($t_{\rm p}\approx 9$ min) as the single peak in the crystallization exotherm for LE/E_EL.

Figures 5d, 5e, and 5f show the heating traces after the isothermal crystallization experiments shown in Figures 5a, 5b, and 5c, respectively. In all cases, melting peaks are evident, indicating that the samples at least partially crystallized during the isothermal crystallization. The fraction of the PLLA block that is crystallized ($\Phi_{\rm c,PLLA}$) was estimated using the equation

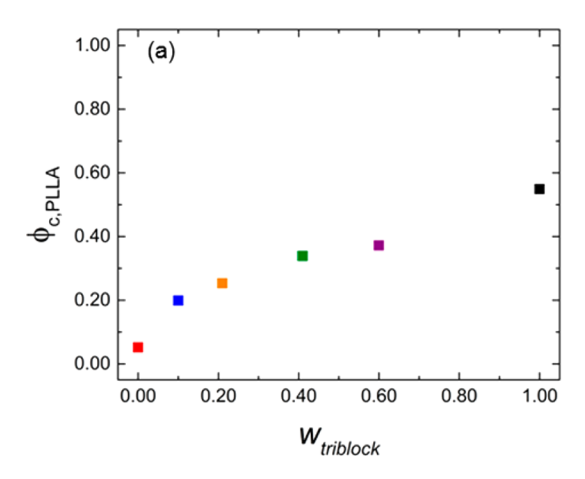
$$\Phi_{c,PLLA} = \frac{H_{\rm m}}{H_{\rm m}^{\infty} w_{\rm PLLA}} \tag{1}$$

where $H_{\rm m}^{\infty}$ is the heat of fusion for an infinite PLLA crystal (93 J/g), 49 $w_{\rm PLLA}$ is the weight fraction of PLLA in the sample, and $H_{\rm m}$ is the measured heat of fusion. Figure 6a shows the estimated $\Phi_{\rm c,PLLA}$ for samples after the isothermal crystallization procedure. The measured difference in $\Phi_{\rm c,PLLA}$ for two samples after 1 h isothermal crystallization indicates that $({\rm LE/E_EL})_{(3.6)}$ developed less crystallinity over the course of 1 h than ${\rm LE/E_EL}$. Furthermore, the observation that $\Phi_{\rm c,PLLA}$ of $({\rm LE/E_EL})_{(3.6)}$ increased with longer crystallization times suggests that the lower crystallinity of $({\rm LE/E_EL})_{(3.6)}$ compared to ${\rm LE/E_EL}$ after 1 h of isothermal crystallization is due to kinetic limitations.

Before discussing the possible origins of these kinetic limitations of crystallization of $(LE/E_EL)_{\langle 3.6\rangle}$, we point out two interesting features regarding the peak melting temperatures. Figure 6b shows the peak melting temperature $(T_{\rm m,peak})$

for the samples after various isothermal crystallization procedures. Regardless of crystallization time or temperature, $T_{\rm m,peak}$ for $(\rm LE/E_E L)_{\langle 3.6 \rangle}$ was lower than the lower temperature melting peak $T_{\rm m,peak,1}$ of LE/E_EL crystallized at the same $T_{c\prime}$ suggesting that the crystallized (LE/E_EL)_(3.6) has thinner lamellar crystals. This result may arise from LE/E_EL being held at T_c for 1 h, which is much longer than is necessary for the sample to fully crystallize as shown in Figure 5a. Therefore, LE/E_EL may have experienced isothermal thickening during the extended annealing period. 51 The second feature of the melting peaks that is worth noting is the observation of double melting peaks after LE/E_EL has been crystallized at lower T_cs (see Figure 5d). Multiple melting peaks are commonly observed for semicrystalline polymers and may be due to the presence of multiple crystal populations⁵² or melt-recrystallization processes.⁵³ If the double melting peak is due to partial melting of the crystals followed by recrystallization, the Φ_{cPLLA} indicated in Figure 6b may be an overestimate. Nevertheless, even if the two melting peaks were deconvoluted and only the low temperature peak was integrated to determine Φ_{cPLLA} , the estimated crystallinity of LE/E_EL would still be greater than $(LE/E_EL)_{\langle 3.6 \rangle}$ under the same isothermal crystallization conditions, and the main conclusions would still hold. Since the origin of the double melting peak is unknown, both the low temperature peak $(T_{m,peak 1})$ and higher temperature peak $(T_{\text{m,peak 2}})$ are included in Figure 6b.

Figures 5 and 6 provide evidence that the crystallization of $(LE/E_EL)_{(3.6)}$ is frustrated compared to LE/E_EL . Considering that LE/E_EL and $(LE/E_EL)_{(3.6)}$ have identical compositions and identical morphologies with nearly the same domain spacing prior to crystallization, the differences in crystallization behavior must be attributed to other factors. The only difference



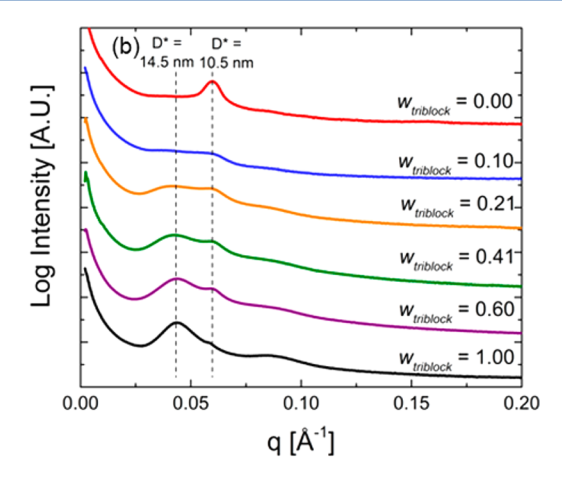


Figure 8. (a) $\Phi_{c,PLLA}$ measured after 1 h isothermal crystallization at 100 °C versus the $w_{triblock}$ of each sample. (b) SAXS pattern taken after 1 h isothermal crystallization at 100 °C and quenching sample to room temperature. Red, blue, orange, green, purple, and black symbols and lines correspond to LE/E_EL, (LE/E_EL)_{⟨1.4⟩,} (LE/E_EL)_{⟨1.4⟩,} (LE/E_EL)_{⟨2.4⟩,} (LE/E_EL)_{⟨2.4⟩,} and (LE/E_EL)_{⟨3.6⟩,} respectively.

between these materials is the chain architecture, which we speculate influences the crystallization kinetics. The bridging and looping PLLA blocks in the multiblock copolymers are topologically constrained due to pinning of both block ends to the PLLA/PE/E_E interface as illustrated in Figure 7. The PLLA blocks in LE/E_EL are all dangling chains with only one end of the blocks pinned to the interface. These dangling chain ends have higher mobility than the interior PLLA blocks of the multiblock copolymer. The restricted chain mobility of the loops and bridges likely encumbers nucleation. Thus, the dangling ends having a higher probability of forming nuclei of critical size, which can then grow into lamellar crystals. Additionally, dangling ends have more mobility and are more likely to attach to an existing crystal face and grow via a secondary nucleation step. Along with the effects of interfacial pinning, crystallization of the interior blocks of $(LE/E_EL)_{(3.6)}$ may further impede the mobility of the blocks. This picture of different rates of nucleation and growth for the dangling chain ends versus interior blocks is supported by the observation of two exothermic peaks in Figure 5c, which suggests two distinct mechanisms with different crystallization kinetics.

This pinning effect may be related to phenomena reported in cross-linked homopolymer systems. For example, previous work on cross-linked poly(cylcooctene) polymers showed that the crystallinity of the samples decreased as a function of crosslink density,54 demonstrating that the molecular weight between cross-links is a critical factor. In the LE/E_EL/(LE/ $E_E L$)_(3,6) system, the molecular weight between the effective cross-linking points is the length of the PLLA block which is approximately 4000 and 8000 g/mol for the dangling ends and (coupled) interior blocks, respectively. The relatively low molecular weight of the blocks might explain why other reports dealing with multiblock copolymer have not documented such dramatic consequences of architecture on crystallization. Chen and co-workers investigated PLLA-PEG (where PEG is poly(ethylene glycol)) triblock and multiblock copolymers and found that the melting enthalpy in the DSC heating ramp was systematically lower for the multiblock copolymers compared to the triblock copolymers. 19 Interestingly, they also found that increasing the length of the PLLA block increased the overall crystallinity of the samples. Koo and coworkers investigated rubbery/semicrystalline multiblock copolymer with poly(ethylene) (PE) blocks and reported that

samples with larger n' required larger supercooling to crystallize during a DSC cooling ramp. Although PE crystallizes much more rapidly than PLLA, apparently varying connectivity still influences crystallization in that system.

This hypothesis is further reinforced by isothermal crystallization experiments performed at $T_{\rm c}$ = 100 °C for 1 h for the LE/E $_{E}L/(LE/E_{E}L)_{\langle 3.6\rangle}$ blends. Figure 8a shows the $\Phi_{\text{c.PLLA}}$ measured after the crystallization procedure as a function of w_{triblock} in the sample. As w_{triblock} increases, the fraction of dangling PLLA blocks also increases, resulting in an increase in $\Phi_{c.PLLA}$. Figure 8b shows SAXS patterns taken on samples that underwent identical isothermal crystallization procedures ($T_c = 100$ °C, 1 h) but were quenched rapidly to room temperature in order to vitrify the sample and preserve the morphology after the crystallization procedure. Focusing on $(LE/E_EL)_{(3,6)}$, which has developed a very small amount of crystallinity after isothermal crystallization, the SAXS pattern shows a peak corresponding to $D^* = 10.5$ nm as well as a very broad and less intense scattering peak at lower q. With increasing $w_{triblock}$ the low q peak intensity grows with a concurrent decrease in the higher q scattering intensity. For LE/E_EL ($w_{\text{triblock}} = 1$), the low q peak ($D^* = 14.5$ nm) is the predominant feature in the scattering pattern. These results indicate that the crystallization process appears to perturb the morphology that was present in the melt. As shown in Figure 3, D^* in the melt (180 °C) is ~9.8 nm for all samples. Upon cooling, in the absence of crystallization, D^* should increase slightly due to the increase in the segregation strength, which explains the peak corresponding to $D^* = 10.5$ nm. As $\Phi_{c,PLLA}$ increases, however, the original morphology appears to be destroyed and the scattering patterns for the blends appear to be a convolution of two peaks, which arise due to coexistence of the unperturbed morphology and the new morphology, which forms after crystallization. Establishing the exact morphology that forms after crystallization will be the subject of future work.

The SAXS data in Figure 8 provide clear evidence that breakout crystallization is occurring in this system. Since distorting the initial mesostructure requires diffusion of the polymer chains, it is important to consider how differences in the molecular weight between the triblock and multiblock copolymer could influence the diffusion of chains and subsequently the crystallization kinetics. Pan and co-workers studied the isothermal crystallization of PLLA of various

Table 3. Summary of Mechanical Properties

sample	$\Phi_{ m c,PLLA}$	$w_{ m triblock}$	E (MPa)	ε_{b} (%)	$\sigma_{\!\scriptscriptstyle m b} \; ({ m MPa})$	$\sigma_{ m yield}$ (MPa)
LE/E_EL	0.06	1.00	253 ± 14	5 ± 3	9.1 ± 3.9	
$(LE/E_EL)_{\langle 1.4 \rangle}$	0.06	0.60	640 ± 107	4 ± 2	19.9 ± 6.3	
$(\text{LE/E}_{\text{E}}\text{L})_{\langle 1.8 \rangle}$	0.02	0.41	619 ± 95	191 ± 178	21.6 ± 9.0	30.6 ± 3.6
$(LE/E_EL)_{\langle 2.4\rangle}$	0.03	0.21	540 ± 47	450 ± 159	18.7 ± 1.4	28.0 ± 2.1
$(LE/E_EL)_{\langle 2.9 \rangle}$	0.01	0.10	624 ± 67	414 ± 114	20.9 ± 1.4	29.1 ± 2.4
$(LE/E_EL)_{\langle 3.6 \rangle}$	0.01	0.00	549 ± 30	632 ± 128	23.5 ± 2.2	27.7 ± 1.2
$(LE/E_EL)_{\langle 1.8 \rangle}$ (annealed)	0.39	0.41	586 ± 27	34 ± 16	20.4 ± 2.1	
$(LE/E_EL)_{\langle 3.6\rangle} \; (annealed)$	0.09	0.00	667 ± 80	422 ± 158	22.0 ± 2.2	31.4 ± 2.6

molecular weights and examined the peak crystallization time $(t_{\rm p})$ for various $T_{\rm c}$ s. They found that $t_{\rm p}$ occurred at ~1 min and ~4 min for 15 and 118 kg/mol PLLA samples, crystallized at $T_c = 100$ °C, respectively. Since t_p roughly corresponds to the crystallization half-time, ⁵⁶ we can estimate that crystallization was completed in 2 min for the 15 kg/mol sample and 8 min in the 118 kg/mol sample. This translates to about 4 times greater time to crystallize when the molecular weight is increased by a factor of 10. In contrast, for our triblock $(M_n =$ 10.5 kg/mol), crystallization at $T_c = 100$ °C is completed in about 18 min. The retardation in the crystallization kinetics of the triblock copolymer compared to homopolymers is likely due to pinning of the PLLA blocks to one interface. Crystallization of the multiblock copolymer, which has 3.6 times the $M_{\rm p}$ of the triblock, has not finished after 3 h at $T_{\rm c}$ = 100 °C, i.e., more than 10 times that required for obtaining maximum crystallinity in the triblock material. These differences in crystallization time are much more dramatic than would be anticipated from the study of homopolymer PLLA of different molecular weight, indicating that differences in the diffusion coefficient of the triblock and multiblock are not the predominant factor causing slower crystallization kinetics.

Mechanical Properties. Uniaxial extensional testing was employed to characterize the mechanical behavior of LE/E_EL, $(LE/E_EL)_{(3,6)}$, and the $LE/E_EL/(LE/E_EL)_{(3,6)}$ blends. A summary of the relevant figures of merit determined from the uniaxial extension experiments including Young's modulus (E), strain at break (ε_b) , tensile stress (σ_b) , and yield stress (σ_{yield}) are included in Table 3. All samples were prepared using a compression molding procedure in which samples were placed on a hot press at $T > T_{\text{m,PLLA}}$ and rapidly cooled to $T \sim T_{\text{g,PLLA}}$ to produce a film from which tensile bars were formed using a punch. In addition, to examine the role of crystallinity on mechanical properties, two samples, $(LE/E_EL)_{(1.8)}$ and $(LE/E_EL)_{(1.8)}$ $E_E L$)_(3.6), were also prepared by a modified procedure that yielded a different thermal history. Films of these two samples were first shaped using the aforementioned compression molding procedure. After this, the samples were left at room temperature for 30 min, followed by annealing under compression on the hot press for 30 min at 100 °C. Samples prepared with the additional annealing step are labeled as "annealed" in Table 3 as well as in the associated figures. We will first discuss the role of $\langle n \rangle$ on mechanical properties by considering the results for the unannealed samples and then discuss the effect of enhancing crystallinity through the annealing process.

Figure 9 shows the engineering stress versus engineering strain behavior of the unannealed samples under uniaxial extension. The compression molding procedure resulted in samples with relatively low crystallinity ($\Phi_{c,PLLA} \leq 0.06$) for all samples, which is attributed to slow crystallization kinetics of

the PLLA domains relative to the cooling rate of the hot press. SAXS measurements taken on the films prior to mechanical testing indicated that long-range order was mostly preserved for all samples since a sharp primary peak and one or more higher order reflections were observed for each of these samples (see Supporting Information). Additionally, since $\Phi_{\rm c,PLLA}$ is relatively low, we assume that mechanical properties are likely unaffected by the small amount of crystalline PLLA present in this set of samples.

Not surprisingly, the mechanical properties are affected by decreasing w_{triblock} (or, equivalently, increasing $\langle n \rangle$). Notably, samples with $w_{\text{triblock}} \leq 0.41 \ (\langle n \rangle \geq 1.4)$ exhibited ductile behavior, while samples with smaller $\langle n \rangle$ (or, equivalently, higher $w_{\rm triblock}$) were brittle. The increase of $\varepsilon_{\rm b}$ with decreasing w_{triblock} implicates the multiblock copolymer and its capability to bridge the PLLA matrix as the origin of the enhanced mechanical properties in this system. The ductile samples $(w_{\text{triblock}} \leq 0.41)$ exhibited a sharp yield stress which corresponded with formation a necked region, with these samples displaying identical values of σ_{vield} (within experimental error). Yielding was followed by a stress plateau associated with further drawing and neck propagation. Two samples, (LE/ $(E_EL)_{(2.9)}$ and $(LE/E_EL)_{(3.6)}$, which had the smallest $w_{triblock}$, also exhibited strain hardening, suggesting that the bridging fraction was sufficient to sustain the stresses associated with the alignment of the chains/microdomains.

Although both the annealed materials were prepared using identical procedures, the crystallinity differed; using DSC, $\Phi_{c,PLLA}$ was found to be 0.39 and 0.09 for $(LE/E_EL)_{(1.8)}$ (annealed) and $(LE/E_EL)_{(3.6)}$ (annealed), respectively. This result is consistent with the isothermal crystallization data. Not surprisingly, polarized optical microscopy (POM) images taken on the films prior to mechanical testing also suggests that (LE/ $E_E L$) $_{(3.6)}$ (annealed) developed less crystallinity than (LE/ $E_E L$)_(1.8) (annealed) during the annealing process (see Supporting Information). Nevertheless, $\Phi_{c.PLLA}$ is significantly higher after the annealing process when compared to the samples that were not annealed (see Table 3). The uniaxial extensional data for both annealed samples is given in Figure 10. Additionally, in order to facilitate comparison between the annealed and unannealed samples, Figure 11 shows the $\varepsilon_{\rm b}$ for all the samples containing different amounts of w_{triblock} .

The stress–strain behavior of $(LE/E_EL)_{\langle 3.6\rangle}$ (annealed), shown in Figure 10b, is very similar to that of the unannealed sample (see Figure 9f). This is likely due to only minor differences in $\Phi_{c,PLLA}$ (0.01 for unannealed and 0.09 for annealed). Additionally, the SAXS patterns are nearly identical for both samples (see Supporting Information). The average measured values of ε_b , σ_b , and σ_{yield} for $(LE/E_EL)_{\langle 3.6\rangle}$ (annealed) and $(LE/E_EL)_{\langle 3.6\rangle}$ agree within experimental error. E, on the other hand, is slightly higher for $(LE/E_EL)_{\langle 3.6\rangle}$

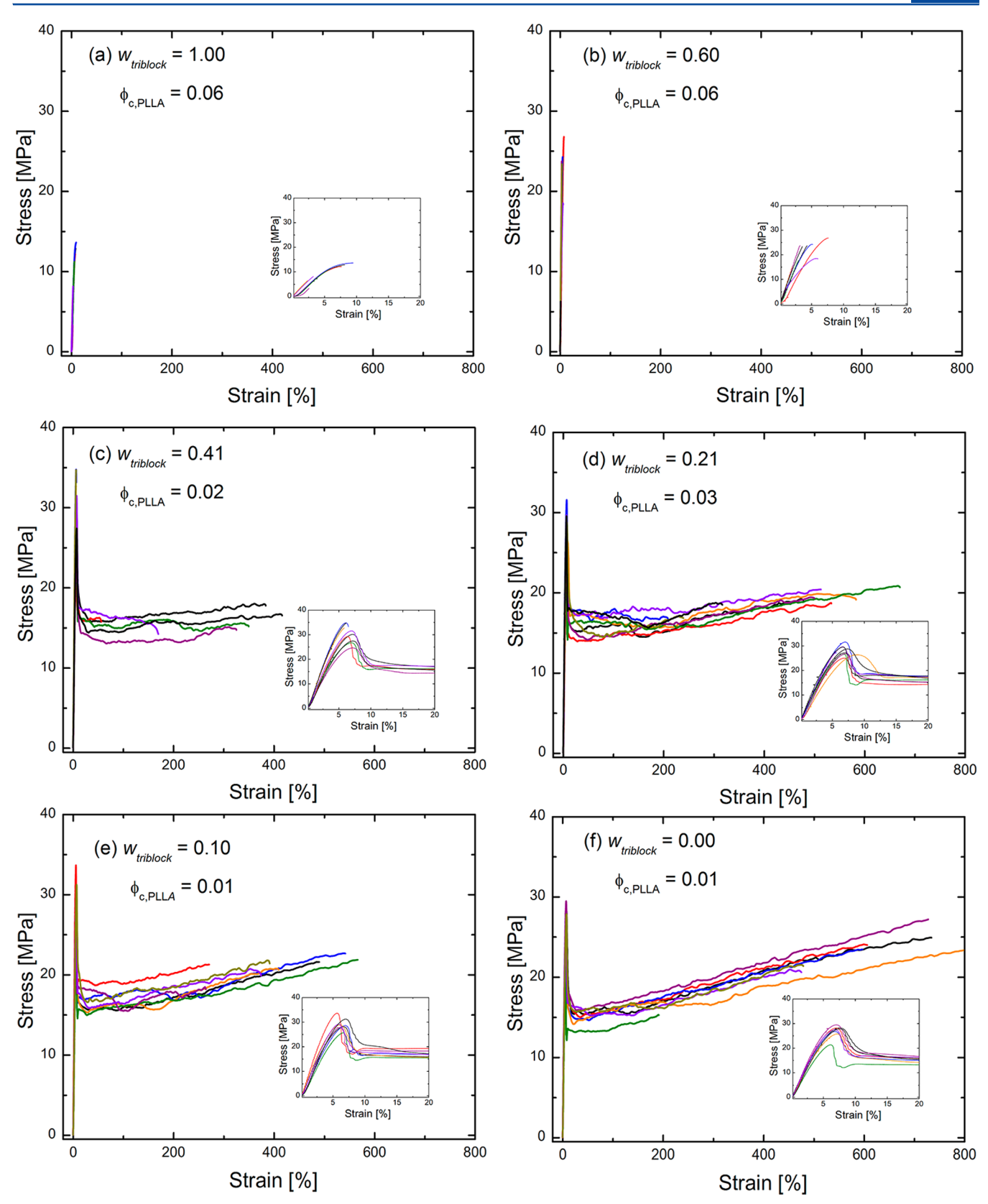
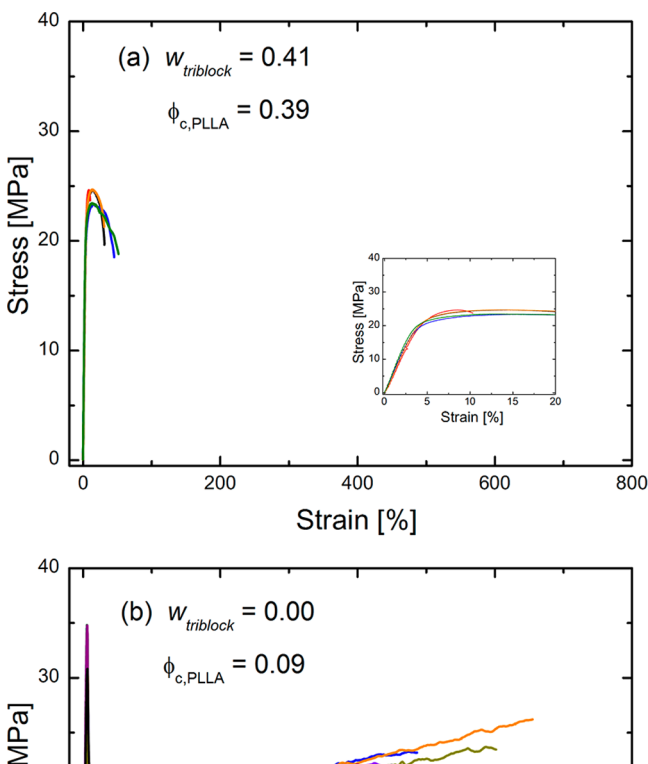


Figure 9. Stress versus strain data from tensile tests. Samples were prepared by hot pressing at 170 °C followed by rapid cooling. $\Phi_{c,PLLA}$ after pressing procedure is listed for each sample. (a) LE/E_EL, (b) (LE/E_EL)_(1.4), (c) (LE/E_EL)_(1.8), (d) (LE/E_EL)_(2.4), (e) (LE/E_EL)_(2.9), and (f) (LE/E_EL)_(3.6).

(annealed), indicating that subtle changes in crystallinity can modulate this parameter. POM images were taken on the films prior to deformation (see Supporting Information). Interestingly, $(LE/E_EL)_{\langle 3.6\rangle}$ (annealed) clearly shows spherulites that are about 5 μ m in size. This provides concrete evidence that crystallization in this case is not confined to the nanodomains



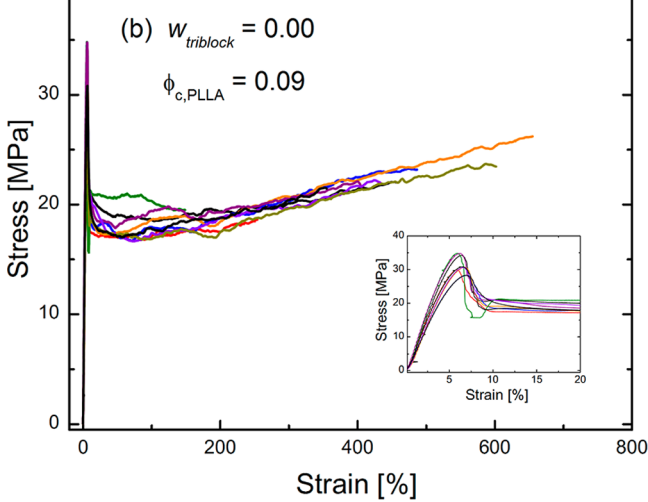


Figure 10. Stress versus strain data from tensile tests on samples which were annealed to enhance crystallinity: (a) $(LE/E_EL)_{\langle 1.8\rangle}$ (annealed) and (b) $(LE/E_EL)_{\langle 3.6\rangle}$ (annealed). Samples were prepared by hot pressing at 170 °C followed by rapid cooling to prepare films. Films were subsequently annealed for 30 min at 100 °C to enhance crystallinity. $\Phi_{c.PLLA}$ after pressing procedure is listed for both samples.

of the block copolymer. Surprisingly, the presence of the spherulites does not seem to influence the mechanical behavior; the stress—strain response of the unannealed (LE/E_EL) $_{(3.6)}$ sample, which did not show the presence of spherulites at the same magnification, is nearly identical.

In contrast to $(LE/E_EL)_{\langle 3.6\rangle}$ which was mostly unaffected by the annealing procedure, the stress—strain behavior of $(LE/E_EL)_{\langle 1.8\rangle}$ (annealed) shown in Figure 10b is very different from that of the unannealed sample shown in Figure 9c. $(LE/E_EL)_{\langle 1.8\rangle}$ (annealed) had a significantly higher amount of crystallized PLLA compared to the unannealed sample $(\Phi_{c,PLLA}=0.02$ for unannealed and $\Phi_{c,PLLA}=0.39$ for annealed sample), and SAXS data taken on $(LE/E_EL)_{\langle 1.8\rangle}$ (annealed) prior to tensile testing revealed that crystallization seemed to destroy the long-range order present in the sample prior to annealing (see Supporting Information). Thus, the changes in mechanical behavior reflect both the crystallinity and changes in morphology, making it challenging to decouple these factors. Unlike the unannealed specimen, $(LE/E_EL)_{\langle 1.8\rangle}$ (annealed)

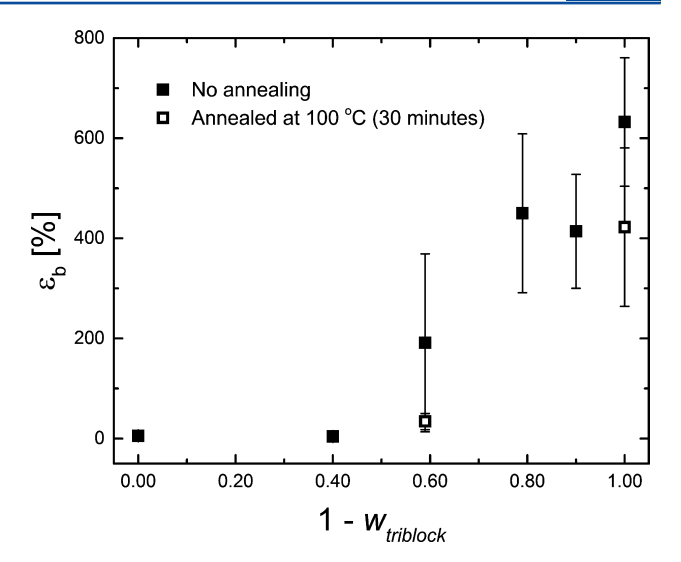


Figure 11. $\varepsilon_{\rm b}$ versus $1-w_{\rm triblock}$ for quenched (closed symbols) and annealed (open symbols) samples.

does not have a sharp yield stress and softens prior to failure. This change indicates that the mechanical response and ultimate failure occur by different mechanisms in the annealed sample. The relatively low $\varepsilon_{\rm b}$ and absence of a sharp yield stress may be due to changes in the chain configurations induced by crystallization, which could reduce the number of bridging blocks. The interior PLLA blocks are most likely to crystallize at nucleation points in closest proximity to the chain. This could induce a looping configuration since PLLA blocks have a high probability of returning to adjacent domains. With further crystallization, the motion of the PLLA blocks is further impeded resulting in an additional increase in the looping fraction. Thus, the mechanical properties are probably dominated by interlamellar slip and/or interlamellar separation occurring within the PLLA crystals. 57

CONCLUSIONS

While increasing $\langle n \rangle$ undoubtedly results in improvements in overall mechanical properties, we have shown that it also results in slower overall crystallization kinetics. We suggest that the reduced rate of crystallization of the multiblock copolymer is due to pinning of the interior blocks to two interfaces which reduces the mobility of the blocks. Our results demonstrate that blending triblock and multiblock copolymers is an effective strategy for optimizing competing properties including the rate of crystallization and overall mechanical toughness in sustainable polymeric materials and gives insight into methods for improving properties of sustainable building blocks by employing multiblock copolymer architectures.

ASSOCIATED CONTENT

S Supporting Information

Additional characterizations and figures. The Supporting Information is available free of charge on the ACS Publications website at DOI: 10.1021/acs.macromol.5b01029.

AUTHOR INFORMATION

Corresponding Author

*E-mail: bates001@umn.edu (F.S.B.).

Notes

The authors declare no competing financial interest.

ACKNOWLEDGMENTS

This work was supported by the National Science Center through the Center for Sustainable Polymers at the University of Minnesota, a Center for Chemical Innovation (CHE-1413862) and through a NSF Graduate Fellowship (Grant No. 0006595 to T.R.P.). SAXS was performed at the DuPont-Northwestern-Dow Collaborative Access Team (DND-CAT) located at Sector 5 of the Advanced Photon Source (APS). DND-CAT is supported by E. I. du Pont de Nemours & Co., The Dow Chemical Company, and Northwestern University. Use of the APS, an Office of Science User Facility operated for the U.S. Department of Energy (DOE) Office of Science by Argonne National Laboratory, was supported by the U.S. DOE under Contract DE-AC02-06CH11357. Parts of this work were carried out in the Characterization Facility, University of Minnesota, a member of the NSF-funded Materials Research Facilities Network via the MRSEC program. We also thank Matthew Irwin, Intaek Lee, and Brandon Adams for their assistance with staining and microtoming TEM samples, mechanical testing, and blend preparations, respectively.

REFERENCES

- (1) Bates, F. S.; Hillmyer, M. A.; Lodge, T. P.; Bates, C. M.; Delaney, K. T.; Fredrickson, G. H. *Science* **2012**, *336*, 434–440.
- (2) Hermel, T. J.; Hahn, S. F.; Chaffin, K. A.; Gerberich, W. W.; Bates, F. S. Macromolecules 2003, 36, 2190-2193.
- (3) Ryu, C. Y.; Ruokolainen, J.; Fredrickson, G. H.; Kramer, E. J.; Hahn, S. F. *Macromolecules* **2002**, *35*, 2157–2166.
- (4) Lee, I.; Panthani, T. R.; Bates, F. S. Macromolecules 2013, 46, 7387-7398.
- (5) Matsumiya, Y.; Watanabe, H.; Takano, A.; Takahashi, Y. *Macromolecules* **2013**, 46, 2681–2695.
- (6) Koo, C. M.; Hillmyer, M. A.; Bates, F. S. *Macromolecules* **2006**, 39 (2), 667–677.
- (7) Cohn, D.; Salomon, A. H. Biomaterials 2005, 26, 2297-2305.
- (8) Spontak, R. J.; Smith, S. D. J. Polym. Sci., Part B: Polym. Phys. 2001, 39, 947–955.
- (9) Lin, J.; Chen, W.; Shen, Z.; Ling, J. Macromolecules 2013, 46, 7769-7776.
- (10) Arman, B.; Reddy, A. S.; Arya, G. Macromolecules 2012, 45, 3247-3255.
- (11) Khanna, V.; Ruokolainen, J.; Kramer, E. J.; Hahn, S. F. *Macromolecules* **2006**, *39*, 4480–4492.
- (12) Xiong, M.; Schneiderman, D. K.; Bates, F. S.; Hillmyer, M. A.; Zhang, K. Proc. Natl. Acad. Sci. U. S. A. 2014, 111, 8357–8362.
- (13) Wanamaker, C. L.; O'Leary, L. E.; Lynd, N. A.; Hillmyer, M. A.; Tolman, W. B. *Biomacromolecules* **2007**, *8*, 3634–3640.
- (14) Martello, M. T.; Burns, A.; Hillmyer, M. ACS Macro Lett. 2012, 1, 131–135.
- (15) Lee, I.; Bates, F. S. Macromolecules 2013, 46, 4529-4539.
- (16) Zhong, Q.; Ren, J.; Wang, Q. Polym. Eng. Sci. 2011, 51, 908–916.
- (17) Ryynanen, T.; Nyaken, A.; Seppala, J. V. eXPRESS Polym. Lett. 2008, 2, 184-193.
- (18) Ojha, U.; Kulkarni, P.; Singh, J.; Faust, R. J. Polym. Sci., Part A: Polym. Chem. 2009, 47, 3490–3505.
- (19) Chen, W.; Luo, W.; Wang, S.; Bei, J. Polym. Adv. Technol. 2003, 14, 245–253.
- (20) Martello, M. T.; Schneiderman, D. K.; Hillmyer, M. A. Macromolecules 2014, 2, 2519–2526.
- (21) Loo, Y.-L.; Register, R. A.; Ryan, A. J. Macromolecules 2002, 35, 2365-2374.
- (22) Nandan, B.; Hsu, J.; Chen, H. J. Macromol. Sci., Part C: Polym. Rev. 2006. 46, 143-172.
- (23) He, W.-N.; Xu, J.-T. Prog. Polym. Sci. 2012, 37, 1350-1400.

- (24) Xu, J.-T.; Yuan, J.-J.; Cheng, S.-Y. Eur. Polym. J. 2003, 39, 2091–2098.
- (25) Hamley, I. W.; Fairclough, J. P. A.; Bates, F. S.; Ryan, A. J. *Polymer* **1998**, 39, 1429–1437.
- (26) Schmalz, H.; Bo, A.; Lange, R.; Krausch, G. Macromolecules 2001, 34, 8720-8729.
- (27) Mahanthappa, M. K.; Hillmyer, M. A.; Bates, F. S. *Macromolecules* **2008**, *41*, 1341–1351.
- (28) Bishop, J. P.; Register, R. A. Macromolecules 2010, 43, 4954–4960.
- (29) Huang, Y.; Pan, P.; Shan, G.; Bao, Y. RSC Adv. 2014, 4, 47965–47976.
- (30) Myers, S. B.; Register, R. A. Macromolecules 2009, 42, 6665-6670.
- (31) Rangarajan, P.; Register, R. A.; Fetters, L. J. *Macromolecules* **1993**, 26, 4640–4645.
- (32) Ho, R.-M.; Chiang, Y.-W.; Lin, C.-C.; Huang, B.-H. Macromolecules 2005, 38, 4769-4779.
- (33) Ho, R.-M.; Lin, F.-H.; Tsai, C.-C.; Lin, C.-C.; Ko, B.-T.; Hsiao, B. S.; Sics, I. *Macromolecules* **2004**, *37*, 5985–5994.
- (34) Zhu, L.; Cheng, S. Z. D.; Calhoun, B. H.; Ge, Q.; Quirk, R. P.; Thomas, E. L.; Hsiao, B. S.; Yeh, F.; Lotz, B. *Polymer* **2001**, 42, 5829–5830
- (35) Myers, S. B.; Register, R. A. Macromolecules 2010, 43, 393-401.
- (36) Nojima, S.; Toei, M.; Hara, S.; Tanimoto, S.; Sasaki, S. *Polymer* **2002**, 43, 4087–4090.
- (37) Quiram, D. J.; Register, R. A.; Marchand, G. R. *Macromolecules* **1997**, 30, 4551–4558.
- (38) Jamshidi, K.; Ikada, Y. Polymer 1988, 29, 2229-2234.
- (39) Garlotta, D. J. Polym. 2002, 9, 63-84.
- (40) Fetter, L. J.; Lohse, D. J.; Richter, D.; Witten, T. A.; Zirkel, A. *Macromolecules* 1994, 27, 4639–4647.
- (41) Siemann, U. Eur. Polym. J. 1992, 28, 293-297.
- (42) Wu, L.; Cochran, E. W.; Lodge, T. P.; Bates, F. S. Macromolecules 2004, 37, 3360-3368.
- (43) Mori, Y.; Lim, L. S.; Bates, F. S. Macromolecules **2003**, *36*, 9879–
- (44) Walker, C. N.; Sarapas, J. M.; Kung, V.; Hall, A. L.; Tew, G. N. ACS Macro Lett. **2014**, *3*, 453–457.
- (45) Ryan, A. J.; Macosko, C. W. Macromolecules 1992, 25, 6277–6283.
- (46) Velankar, S.; Cooper, S. L. Macromolecules 1998, 31, 9181–9192.
- (47) Velankar, S.; Cooper, S. L. Macromolecules 2000, 33, 395-403.
- (48) Watanabe, H.; Matsumiya, Y.; Sawada, T.; Iwamoto, T. *Macromolecules* **2007**, *40*, *6885*–*6897*.
- (49) Tsuji, H.; Ikada, Y. Polymer 1995, 36, 2709-2716.
- (50) Hoffman, J. D.; Weeks, J. J. J. Res. Natl. Bur. Stand. Phys. Chem. 1962, 66, 13-28.
- (51) Hoffman, J. D.; Weeks, J. J. J. Chem. Phys. 1965, 42, 4301.
- (52) Cocca, M.; Lorenzo, M. L.; Di Malinconico, M.; Frezza, V. Eur. Polym. J. 2011, 47, 1073–1080.
- (53) Shieh, Y.; Liu, G. J. Polym. Sci., Part B: Polym. Phys. 2006, 45,
- (54) Liu, C.; Chun, S. B.; Mather, P. T.; Zheng, L.; Haley, E. H.; Coughlin, E. B. *Macromolecules* **2002**, *35*, 9868–9874.
- (55) Pan, P.; Kai, W.; Zhu, B.; Dong, T.; Inoue, Y. Macromolecules 2007, 40, 6898-6905.
- (56) Lorenzo, A. T.; Arnal, M. L.; Albuerne, J.; Müller, A. J. Polym. Test. 2007, 26, 222–231.
- (57) Galeski, A. Prog. Polym. Sci. 2003, 28, 1643-1699.